Front. Earth Sci. 2022, 16(4): 876−889
https://doi.org/10.1007/s11707-021-0964-7

RESEARCH ARTICLE

Effects of offshore artificial islands on beach stability of sandy shores: case study of Hongtang Bay, Hainan Province

Songzhe LI[1], Biao LV[2], Yunping YANG (✉)[1,2], Yanhua YANG[2], Chenyang WANG[2]

1 State Key Laboratory of Hydraulic Engineering Simulation and Safety, Tianjin University, Tianjin 300072, China
2 Key Laboratory of Engineering Sediment, Tianjin Research Institute for Water Transport Engineering, Ministry of Transport, Tianjin 300456, China

Abstract Artificial island-type reclamation often exerts certain impacts on near-shore sandy shoreline resources and coastal ecological landscapes. The relationship between artificial islands and offshore beach evolution has attracted considerable attention in coastal protection and engineering construction. In this study, we consider Hongtang Bay in Hainan Province, China, as the research object. We adopted the Gao-Collins model to investigate the substrate transport trend in this sea area based on the analysis of the measured hydrologic and sediment data. The shore section from Nanshanjiao to Hongtangling (Taling), including the flat and straight shore sections, is dominated by the lateral transport trend of the vertical shore. The near-shore water has a strong lateral sediment transport capacity, while the outer deep-water area exhibits a sediment transport trend consistent with the tidal current movement. Using multi-year topographic data, the shoreline and seabed alterations in Hongtang Bay were analyzed, and the LITLINE beach evolution model was adopted to simulate the effects of three artificial island layouts with different island filling areas, offshore distances, and plan forms on the near-shore shoreline deformation. The results obtained indicate that the artificial island arrangement with a large offshore distance and a small area has relatively substantial advantages, such as minimizing the adverse effects of artificial island implementation on the near-shore beach.

Keywords offshore artificial island, stability analysis, beach evolution, Hongtang Bay, Hainan

1 Introduction

Since the 1970s, coastal countries in Europe and the United States have actively explored the artificial island mode of port construction to realize safe port development and enhance coordination functions via artificial island construction (Zhang et al., 2011). The construction of artificial islands, such as Palm Jumeirah (Amrousi et al., 2019), Peninsular Malaysia (Chee et al., 2017), the west bank of the Seine River (Rabionet et al., 2008), the west coast of Beidai River (Luo et al., 2016), and Pulau Jerejak (Chee et al., 2017) promote the economic and social development of a country or a region, especially through tourism. The effect of artificial islands on beaches is similar to that of offshore dikes (island). In the wave shadow area behind the breakwater, sedimentation and beach erosion are triggered by the weakening of dynamic forces and strong dynamic forces on both sides of the breakwater, respectively (Lu et al., 2009; Zhu et al., 2019). To determine whether a sand spit or tombolo is formed, prior studies have primarily focused on the scale of sedimentation behind the dike (Walker and Rana, 1999). In fact, the greatest threat from artificial islands to adjacent beaches is continuous erosion on both sides of the beach. Owing to the different sizes, offshore distances, and relative locations of artificial islands, adjacent beaches mainly form two types of protrusions: sandy headlands and tied bars, which influence the evolutionary trend of the nearby beaches (Sheng et al., 2016). Coastal areas are affected by a combination of watersheds, sea tides, waves, and typhoons, thereby making the evolution of near-shore beach morphology a more complex process (Ma et al., 2019; Pang et al., 2021).

Compared with the conventional method of enclosing and creating land by relying on the existing coast to advance seaward, the construction of offshore artificial islands should focus on factors such as the interactions between artificial islands and the marine environment, as well as the evolution of coastal dynamic geomorphology. Several factors affect the stability of offshore or near-shore artificial islands, such as strong tidal effects (Hou

Received June 14, 2021; accepted December 2, 2021

E-mail: yangsan520_521@163.com

et al., 2017), wave current superposition (Kuang et al., 2019), and typhoons (Yang et al., 2019). Different artificial islands exert varying impacts on the marine dynamic conditions, sediment transport, and beach environment in the post-project waters owing to the differences in size, offshore distance, and location. For example, the establishment of an artificial island at the mouth of the Tanghe River in Qinhuangdao City did not increase the sediment siltation near the project area at the estuary, under the implementation of river dredging; however, the sediment siltation is reduced under the influence of the dredging project and diversion effect of the shuttle-shaped island (Sheng et al., 2016). In a study on coastal improvement projects from Yanghekou to Daihekou in Qinhuangdao, it was inferred that the influence of artificial islands on tidal currents when co-existing with coastal improvement projects is a nonlinear superposition of the two cases acting alone; hence, a nonlinear relationship exists between them (Kuang et al., 2019). After the completion of the South China Sea Pearl Artificial Island in Haikou Bay, the beach formed a tongue-like shoreline projecting to the sea, with coastal erosion occurring on both sides, which can be controlled or restored by engineering measures, such as beach sand replenishment (Shi et al., 2015). After the completion of Ridao Island in Hainan Province, the beach in the shadow area of the island silted upward, with a total siltation length and width of approximately 1500 and 370 m, respectively, and significant erosion occurred on the north-east and south-west sides of the island (Li et al., 2019a). After the Haiyang artificial island was completed, the entire surrounding area was slightly silted up, thereby maintaining the state before construction. The north and south sides of the artificial island are always in a state of micro-scouring; hence, no continuous island sand dam will be formed. Furthermore, the local areas on the east and west sides are also in a micro-scouring state (Yue et al., 2008).

Sandy beaches are important geomorphic units in coastal zones. However, 70% of sandy shores are severely eroded by factors such as the natural environment and human activities (Sun et al., 2015; Zhao, 2014). China's coast has also been subject to significant erosion; the length of China's sandy (gravel) shoreline has been declining continuously, with a cumulative reduction of approximately 46.5% from 1980 to 2014 (Hou et al., 2016). The intensity and range of erosion and deposition of near-shore beaches caused by the construction of artificial islands have always been considered in the construction of reefs and islands. The coast of the Hainan Province of China comprises the geological conditions of sand, rock, and sandy gravel. The differences in shoreline sediment composition and dynamic environment make the influence of artificial islands on beaches vary significantly. In this study, the Hongtang Bay area at the southern end of Hainan Province, China, was selected to study the impact of different types of artificial islands on the near-shore beaches and to provide a reference for the construction of artificial islands near the sandy beaches of open sea areas. In this study, we consider the shoreline of Hongtang Bay, Hainan Province, as the research area, and employ a mathematical model of beach evolution, based on the analysis of beach sediment transport and beach evolution to study the counterbalance between the different types of artificial island layouts and beach evolution.

2 Study area and environmental conditions

2.1 Study area

Hongtang Bay is located at the southern end of the Hainan Province, China. Its nearby sea area is not covered by offshore sandbar islands and has suitable water depth conditions. Hongtang Bay's shoreline is smooth, except for the headlands on the east and west sides, and its area is shallower than 5 m. For the flat and straight shore sections, it is a long and narrow zone distributed parallel to the shoreline, with a width of 400–600 m. Isobaths in the area are deeper than 10 m, exhibiting a deflection from Nanshanjiao to the south-east and west of Sanya Bay near Ximao Island. Specifically, the water depth gradually becomes shallower from west to east, with an angle of approximately 40° between the 5 and 20 m isobaths (Fig. 1).

2.2 Wind-wave characteristics

Hongtang Bay is an open bay with a negligible tidal difference and narrow intertidal beach width, and its wave-breaking zone does not migrate significantly with the tide level. In addition, it has a negligible near-shore current velocity, and the tidal current has a weak effect on the shore beach and its submerged slope. The sediment content of the sea area is small, and without a source for foreign sediments, the sediment transport along the coast is small. The waves in the Hongtang Bay Sea area were dominated by wind waves. The normal and subnormal wave directions of the wind waves were SE and SSE with frequencies of 19% and 12%, respectively. The normal and subnormal wave directions of the surge waves were S and SSW with frequencies of 14% and 7%, respectively. The directions with the largest sum of wind and surge wave frequencies were SE and S, with frequencies of 20% and 19%, respectively, followed by SSE, with a frequency of 15% (Fig. 2).

3 Data and methods

3.1 Data

The study derived wave and wind field data of the study

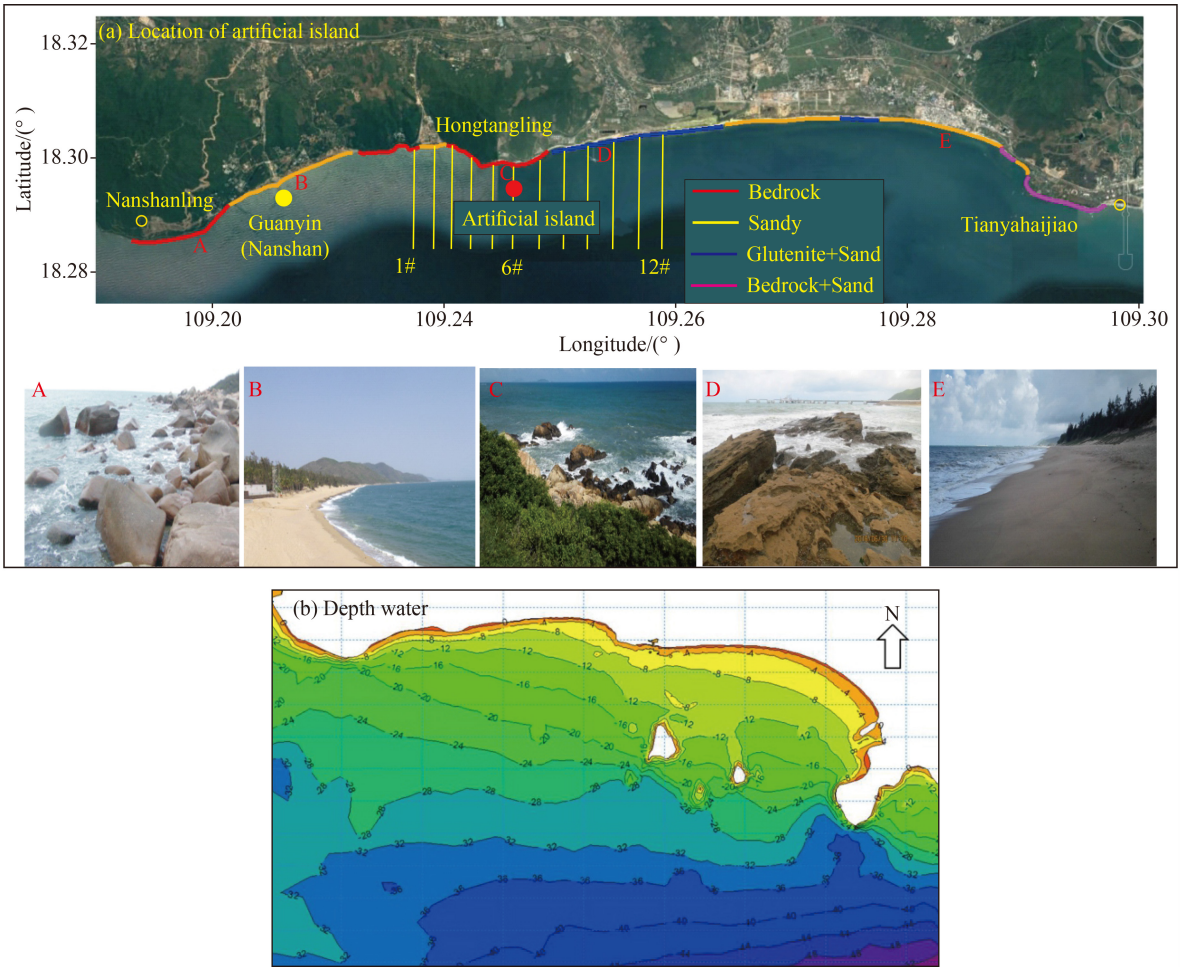

Fig. 1 Study area and representative cross-sections.

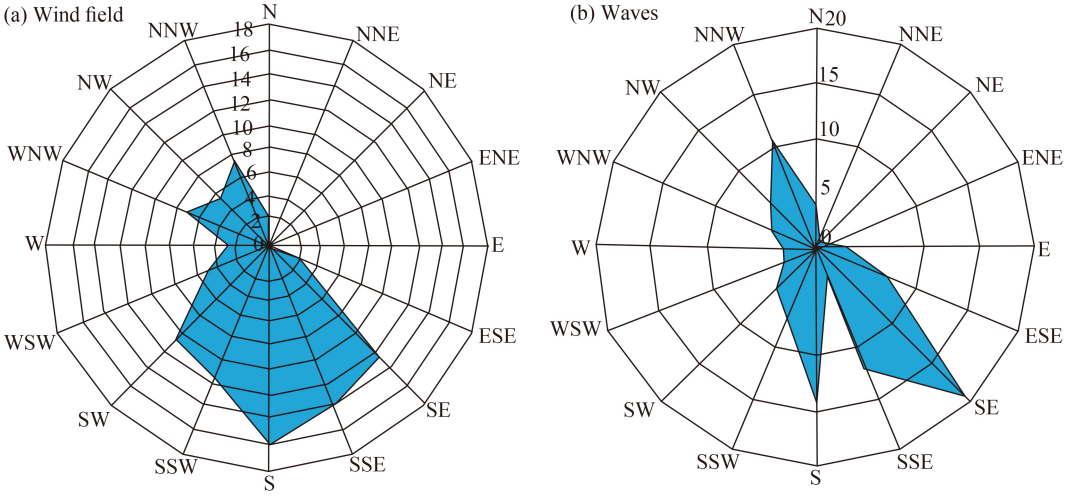

Fig. 2 Wind-wave rose chart.

area from the National Meteorological Administration. This study also collected the riverbed substrate data of Hongtang Bay in 2016, including the riverbed material grain size and riverbed composition, to analyze the bottom sediment transport trend of the sand in Hongtang Bay. In addition, the electronic navigational charts of Hongtang Bay were collected, and the electronic charts for 1987, 1996, 2008, 2015, and 2019 were obtained to analyze the shoreline long-period changes in Hongtang Bay. The actual topographic data of Hongtang Bay were collected to analyze the changes in riverbed sections in the artificial island and nearby areas in 1960, 2013, 2016,

and 2019. The experimental scale was between 1:50000 and 1:100000.

3.2 Methods

The software utilized for the analysis of grain size trends in this study area was a program based on the Gao–Collins method (1994). Since its introduction in 1994, the Gao–Collins model has been widely utilized to simulate sediment transport trends in coastal areas, such as the Chanthaburi Coast in Thailand (Wang et al., 2020) and Laizhou Bay in China (Su et al., 2016).

The difference in the planar distribution of grain size parameters can be adopted to invert the net sediment transport trends because regular changes in grain size parameters along the transport direction often occur during sediment transport. Gao and Collins (1992) proposed that if the three grain size parameters of the sorting coefficient (σ), mean grain size (μ), and skewness (Sk) between any two sampling points A and B satisfy the following relationship, then a grain size trend vector between the two points can be defined:

$$\begin{aligned} &\sigma_A < \sigma_B, \quad \mu_A < \mu_B, \quad Sk_A > Sk_B; \\ &\sigma_A > \sigma_B, \quad \mu_A < \mu_B, \quad Sk_A < Sk_B. \end{aligned} \tag{1}$$

The sum of the trend vectors of each sampling point is the resultant vector, and its ordered distribution represents an anisotropic feature related to the net sediment transport direction, which can be adopted to determine the trend of net sediment transport. The specific operation steps are as follows.

① All sampling points are compared to determine all trend vectors of grain size, and the characteristic distance Der (usually the maximum sampling distance) is utilized to measure whether two sampling points are "adjacent".

② The resultant vector is obtained from the following equation:

$$\vec{R}(x,y) = \sum_1^n \vec{r}(x,y), \tag{2}$$

where $\vec{r}(x,y)$ represents the trend vector for each sampling point, and n is the total number of trend vectors.

③ All vectors are averaged for the smoothing process to remove "noise" from the resultant vectors as follows:

$$\vec{R_m}(x,y) = \frac{1}{K+1}\left[\vec{R}(x,y) + \sum_1^k \vec{R_j}(x,y)\right], \tag{3}$$

where R_j, k, and $\vec{R}(x,y)$represent the resultant vector, the total number of adjacent sampling points, and the smoothed trend vector, whose planar distribution image represents the sediment transport patterns, respectively.

3.3 Beach evolution model

The basic assumption in the LITLINE model is that the longshore sand transport occurs uniformly over the beach profile from the berm height DB down to the depth of the closure Dc (DHI, 2012). The LITLINE model is still widely used to simulate and predict large-scale and long-term beach evolution, owing to its fast computational speed (Zuo et al., 2016; Lin 2017; Wang et al., 2012; Prasad et al., 2020).

The governing equation of the LITLINE shoreline evolution model is based on the law of conservation of mass, which calculates the unit volume change between the two control points, shoreward and offshore, based on the sediment continuity equation, and relates it to the shoreline change, expressed as

$$\frac{\partial y_c(x)}{\partial t} = -\frac{1}{h_{act}(x)} \times \frac{\partial Q(x)}{\partial x} + \frac{Q_{sou}(x)}{h_{act}(x)\Delta x}, \tag{4}$$

where t is time, $y_c(x)$ denotes the distance from the shoreline to the baseline, $h_{act}(x)$ is the effective beach profile elevation, $Q(x)$ is the coastal sediment transport, x denotes the coast location, Δx is the coastal discrete step length, and $Q_{sou}(x)$ represents the sediment source/sink term.

This shore section had special topography and shoreline characteristics—the model range was from the bedrock shoreline of Nanshan Port in the west, to the bedrock shoreline on the west side of the Xiaoqi Port in the east, including the sandy shoreline at the Nanshan and Tianyahaijiao. Therefore, a sufficient buffer shore section length was reserved on the east and west sides. The simulation range was approximately 25 km, and the shoreline was divided into a total of 1250 calculation units with 20 m intervals. The results of the measured underwater topography and substrate sampling in the sea area were used to analyze the topography, shoreline, and sediments. In addition, the bedrock shore section was solidified.

4 Results

4.1 Characteristics of sediment transport

Substrate samples were obtained from the Hongtang Bay area in October 2013. The near-shore substrate sediment obtained from the Hongtang Bay sea area was relatively coarse in grain size (Fig. 3(a)) and dominated by coarse sediment with grain sizes greater than 0.5 mm. Among these samples in the shore section from Hongtangling to Maling, excluding those near the East Cape (Tianyahaijiao Cape), the area shallower than 5 m also had a relatively coarse and unevenly distributed grain size, with a median grain size mostly larger than 0.3 mm and locally larger than 1.3 mm. The average sediment particle content was greater than 90% (Fig. 3(b)). In the area deeper than 5 m, the grain size gradually became finer, as the sand distributed was mostly fine or silty. The median grain size was smaller than 0.1 mm, and the

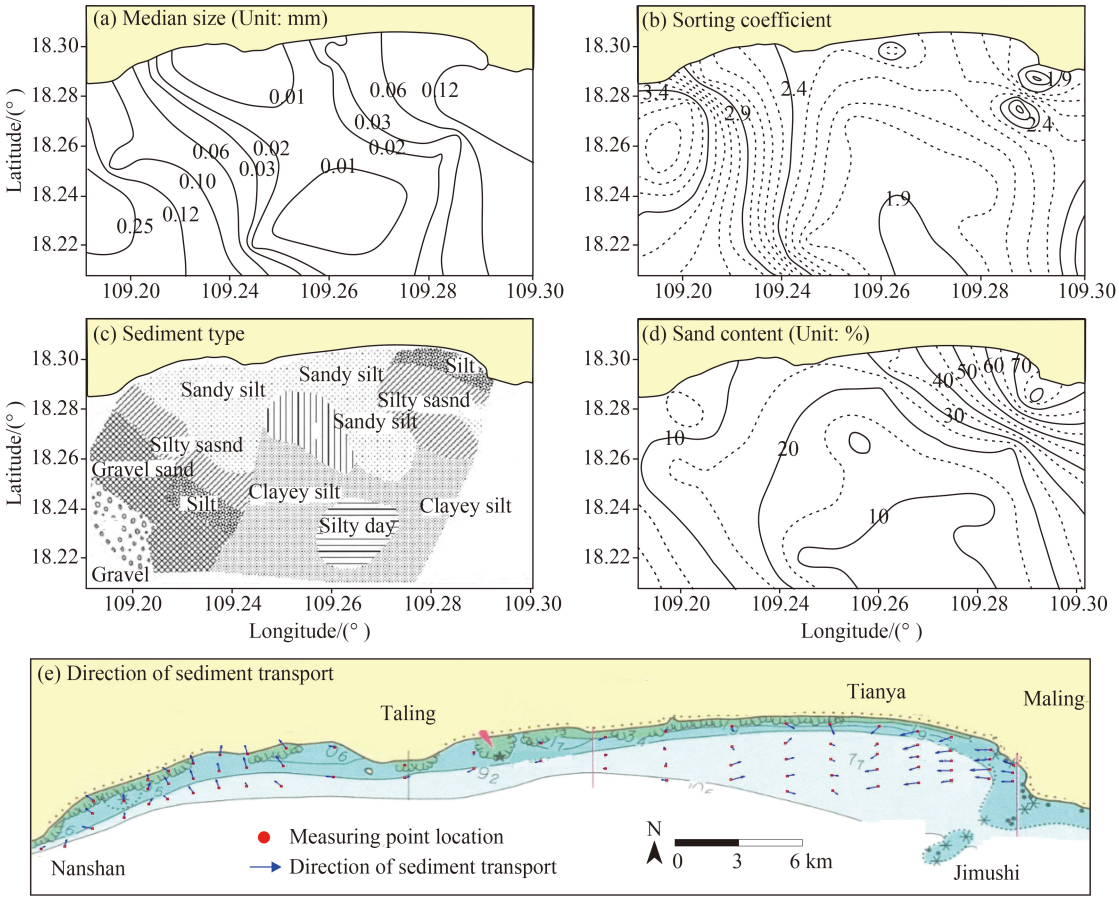

Fig. 3 Key sediment parameters and transport directions in the Hongtang Bay region.

content of silty sediment particles was approximately 20%–35% (Fig. 3(c)).

The Gao–Collins grain size trend analysis method was adopted to analyze the transport trend of the surface substrate in the near-shore area of Hongtang Bay (Fig. 3(d)). It demonstrated that the transport trend of sediment in Hongtang Bay was dominated by the incoming sediment from the sea or the shore beach, with waves as the major controlling force. The transport trend of the sediment samples at the Tianyahaijiao headland bay was stronger under the refraction of waves, while it weakened from the headland bay to the flat and straight shore section in the west and gradually changed to a lateral transport trend perpendicular to the shoreline. The lateral transport trend from Nanshanjiao to Hongtangling was dominated by a lateral transport trend vertical to the shore. The flat and straight shore section was dominated by a lateral transport trend vertical to the shore, which is consistent with the dynamic environment and topographic characteristics of the wave-controlled shore. In terms of lateral sediment transport performance, the water near the shore exhibited a strong sediment transport capacity, thus reflecting the effect of wave changes on the scouring and silting of the near-shore beach. The offshore deep water exhibits a sediment transport trend that is consistent with tidal movement.

4.2 Characteristics of shoreline changes

Shoreline information extracted from remote sensing imagery in 1987, 1996, 2008, 2015, and 2019 was used to analyze shoreline changes along the shore section from Nanshanjiao to Tianyahaijiao (Fig. 4).

1) The west Hongtangling–Nanshanling shore section had a relatively large erosion amplitude, with the local shoreline eroded backward by approximately 50 m, compared to the shoreline in the 1980s. This is primarily related to the submerged topographic features and wave dynamics of the open sea. The submerged topographic slope of this shore section was significant (1/6–1/25). The 10 m isobath was distributed along the shore, and the 20 m isobath was adjacent to Nanshanjiao, where the water was deep and the waves were large, and the wave impact on the beach was stronger. However, along this shore section, the mostly distributed beach rocks provided some resistance to waves; therefore, the beach erosion here was limited. Presently, beach rocks are mostly exposed on the beach surface to form seaside escarpments, and they may be affected by more erosion once the underlying sand layer of the beach rock collapses due to wave erosion.

2) At Tianyahaijiao on the eastern side of the coastline

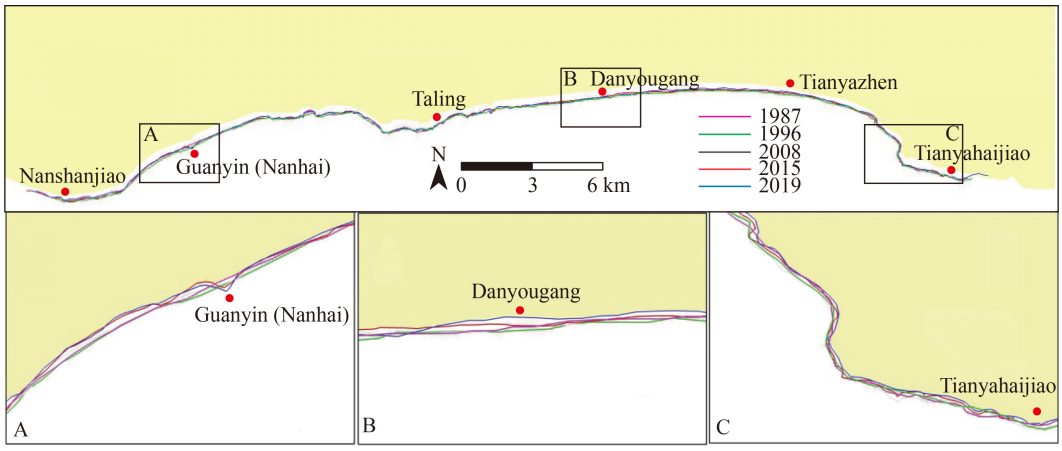

Fig. 4 Shoreline changes.

from Maling to Hongtangling, owing to the sheltering effect of the Jimushi submerged reefs and beaches, the waves were relatively weak, and the overall change in the shoreline was relatively insignificant. The central shoreline (Danyougang) was in a high-energy environment with strong surf action and scoured sediment from the sand bar was transferred to the sea, thereby resulting in shoreline erosion, with an annual erosion range of approximately 2 m. The western bedrock hills were close to the coast, with steep slopes, and the shoreline was eroded under strong tidal waves. However, because of the distribution of coral reefs underwater, the wave energy was partially weakened; hence, the beach was eroded by approximately 30 m.

4.3 Changes in seabed scouring and silting

Twelve longitudinal sections of the riverbed were selected (Fig. 1). The changes in bathymetry for each period in 1961 (chart), 2013, 2016, and 2019 are illustrated for each section (Fig. 5), and the main characteristics of the changes are provided as follows.

1) Each section was in a scouring state, and the water depth of each section varied between 0.46 and 0.92 m, from 1961 to 2013.

2) In the range of 0.0–2.0 km, primarily concentrated in shallow waters less than 10 m, scouring was more significant, and the maximum depth change from 1961 to 2013 was approximately 2.20 m. In the range of 2.0–4.0 km, the maximum depth change from 1961 to 2013 was approximately 0.72 m. In the range of 4.0–6.0 km, scouring became relatively small, and the depth change was between 0.18 m and 0.61 m. Therefore, the intensity of near-shore scouring was greater than the magnitude of scouring and silting in distant waters, which occurred primarily because near-shore waters were in the zone of strong wave action and active lateral transport of sediment movement.

3) From the change in the water depth of the cross-sections in recent years, cross-sections 1#–6# in 2013–2016 exhibited a general scouring state, while cross cross-sections 7#–10# demonstrated slight siltation. The Cross-section 1# in 2016–2019 was scoured by approximately 0.16 m, and the rest of the cross-sections were mostly in a slight siltation state. 7#–10# section appeared as the bulge part, primarily owed to the Sanya New Airport Industrial Park construction, typhoons, and other activities affecting coastal sediment transport. The coastal sediment transport direction in the cross-sectional covered area was westward (Fig. 3). The typhoon path is consistent with the sediment transport direction and is in the mapping area of the airport industrial park, making irregular bulges appear in the cross-sections of 7#–10#.

4) On a long time scale, the beach of this sea area was subjected to wave actions in the SW-SE direction and receded under different degrees of erosion. The shore section from Tianyahaijiao to Nanshanling and its submerged shore slope scouring and silting dynamics were consistent with those of other adjacent bays. When the sea level rose to approximately the current sea level, the source of the marine sediments decreased. In addition, coupled with the fact that there were no large rivers entering the sea in the vicinity of this sea area, the land source sediment was limited. Under the action of waves, the beach section was eroded and receded. Recently, a few areas of the sea have been silted to a certain extent, but the overall extent of siltation is relatively small.

By analyzing the variation in water depth at different distances offshore of each section (Fig. 6), the scouring in the range of 0–2 km near shore during 1961–2013 was significant, and the scouring amplitude was slowed down toward the sea, among which the near-shore scouring amplitude at the location of cross-section 4#–6# was higher than those at other sections. From 2013 to 2019, with the transition from Nanshanjiao to Tianyahaijiao, the overall variation in water depth in the ranges of 0–2, 2–4, and 4–6 km near shore gradually changed from deepening to siltation, where the variation was relatively small in the area of cross-sections 4#–6#, and the magnitude of water depth siltation was relatively large at the location of cross-section 6# in the range of 4–6 km.

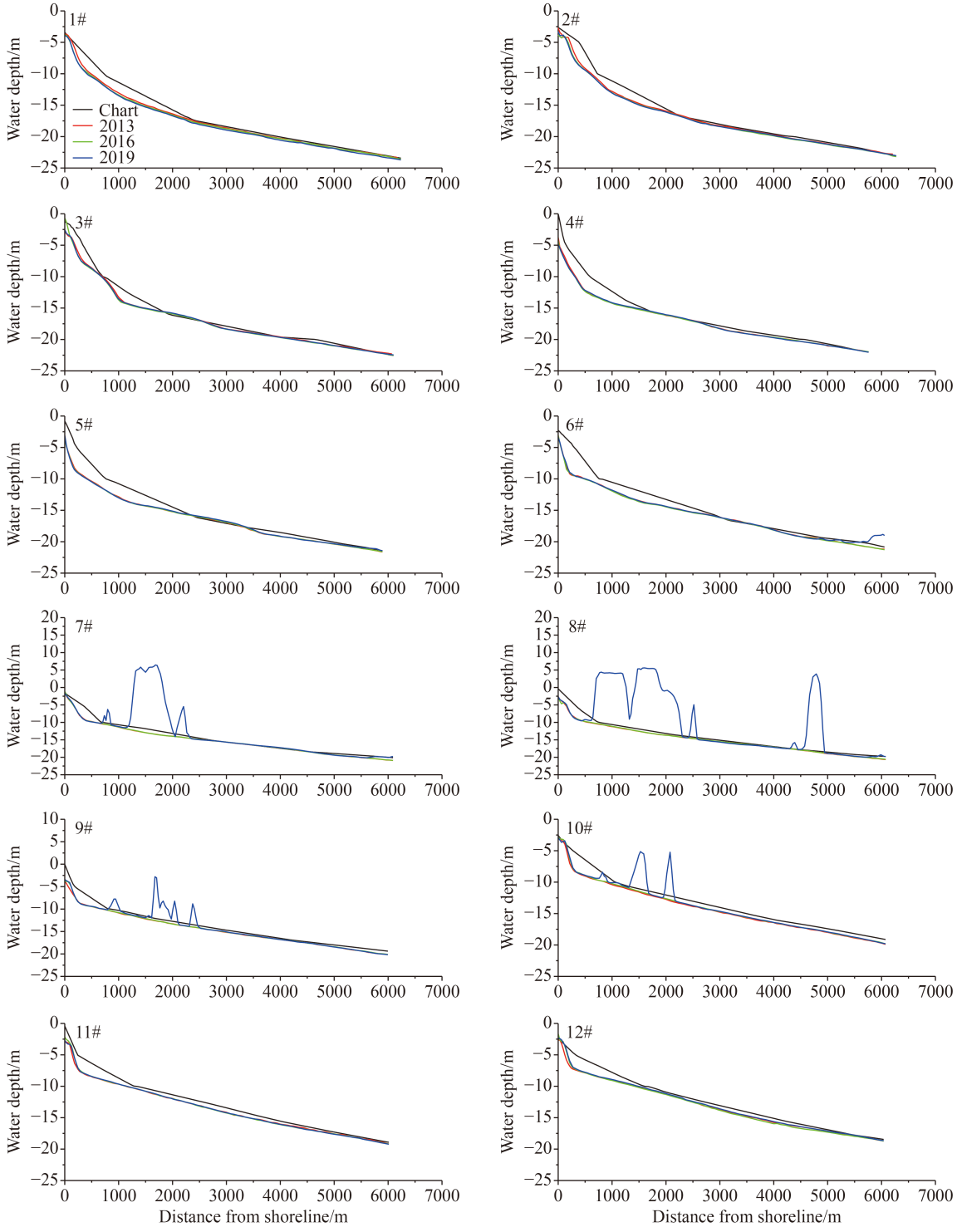

Fig. 5 Longitudinal variations in cross-sections.

4.4 Influence of artificial island construction on the evolution of hydrodynamics

Based on the SWAN model, a twofold nested calculation scheme was adopted to establish a numerical calculation model for near-shore wave propagation deformation. In addition, the wave propagation deformation process of waves in the main wave direction (SSE-W), which occurs once every two years in the Hongtang Bay sea area, from the deeper waters to the near shore of the project, was numerically calculated. Waves in the SSE and SSW directions were the major control waves of coastal and lateral sediment transport in the Hongtang Bay sea area. The effective wave height distribution and wave field

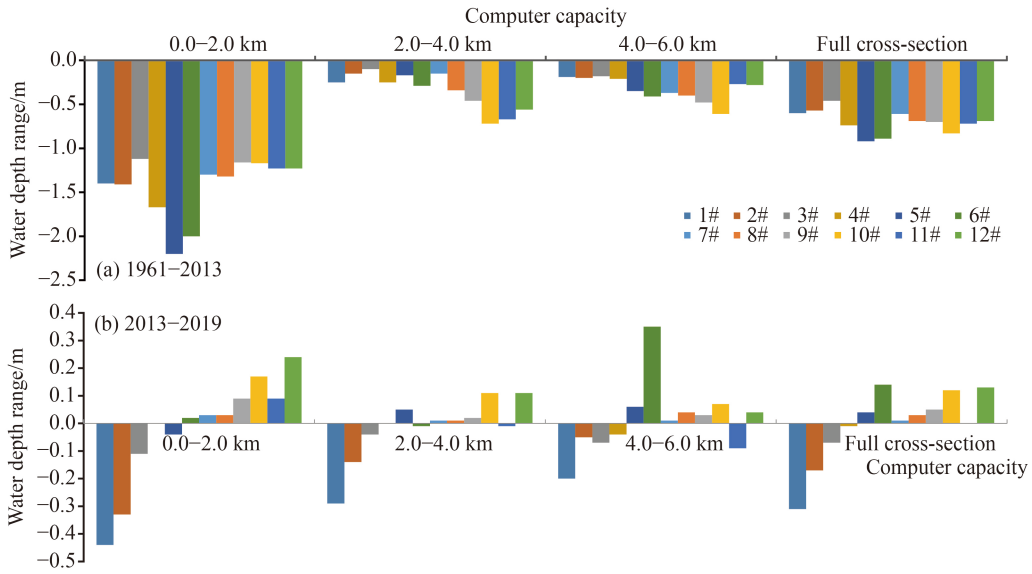

Fig. 6 Distance from shore and variation in water depth at the cross-sections.

map of waves in the main wave direction (SSE-SSW) that occur once every two years are illustrated in Fig. 7, and the results of the wave mathematical model calculations are as follows.

1) In the sea area near Tianyahaijiao, the effective wave heights of the 5 and 10 m isobaths were reduced because of the influence of the artificial island. Under the action of waves in the SSW direction, the effective wave height was reduced by 5%–25%, with a wave deflection of approximately 13°. Under the action of waves in the S direction, the effective wave height was reduced by 1%–15%, with a wave deflection of approximately 10°. Under the action of waves in the SSE direction, the effective wave height was reduced by 1%–8% with a wave deflection of approximately 6°.

2) In the sea area near Nanshan, the effective wave heights of the 5 m and 10 m isobaths were reduced owing to the influence of the artificial island. Under the action of waves in the SSW direction, the effective wave height was reduced by 2%–21%, and the wave direction was deflected by approximately 8°. Under the action of waves in the S direction, the effective wave height was reduced by 7%–35%, and the wave direction was deflected by approximately 10°. Under the action of waves in the SSE direction, the effective wave height was reduced by 14%–46%, and the wave direction was deflected by approximately 12°.

3) In the area behind the artificial island, the effective wave heights of the 5 and 10 m isobaths were reduced owing to the influence of the artificial island. Under the action of waves in the SSW direction, the effective wave height was reduced by 29%–54%, and the wave direction was deflected by approximately 21°. Under the action of waves in the S direction, the effective wave height was reduced by 19%–57%, and the wave direction was deflected by approximately 25°. Under the action of waves in the SSE direction, the effective wave height was reduced by 11%–54%, and the wave direction was deflected by approximately 20°.

In general, because artificial islands are offshore structures in the direction of incoming waves, the waves in the sea behind the artificial island varied significantly. The wave height on the north-west side of the artificial island decreased under the action of waves in the SSW direction, and the wave height on the north side of the artificial island decreased under the action of waves in the S direction. In addition, the wave height on the north-east side of the artificial island decreased under the action of waves in the SSE direction, and the direction of wave propagation was slightly altered.

5 Discussion

5.1 Impacts of artificial islands on the surrounding sea and shoreline erosion and siltation

Based on the tidal-wave sediment mathematical model (refer to Chen 2016, for the modeling process), this study adopted the grid method to calculate the distribution of seawater erosion and siltation after the construction of the new Sanya airport artificial island. The maximum scour thickness on the south-west side of the artificial island was 0.40 m, and the scour intensity of the channel between the north-east side and the artificial island of the industrial park can reach 1.50 m. In addition, on the south side of the artificial island of the airport, the maximum scour thickness reached 1.30 m. The maximum scour thickness between the artificial island of the industrial park and the beach was approximately 0.38 m (Fig. 8).

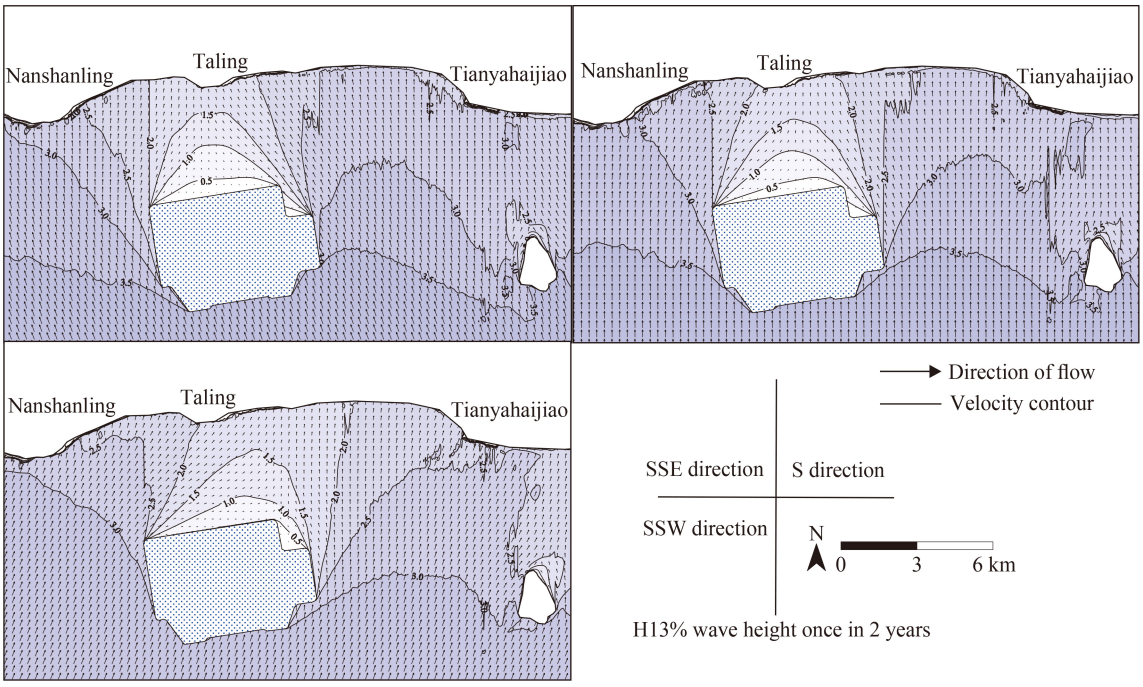

Fig. 7 Contour distribution of different types of wave heights.

5.2 Analysis of the impact of different arrangements of artificial islands on the beach

Based on different island filling areas, offshore distances, and plane morphologies, the artificial island plane layouts were divided into 11 layout schemes in three types (Fig. 9). 1) Layout schemes of different plane morphology types: layout scheme (LS) 1 is the basic scheme (area: 24 km^2, offshore distance: 3.1 km). LS 2 rotates the basic scheme appropriately, and the trend is parallel to the mainstream direction. LS 9 creates an opening in the basic scheme (opening distance of 1 km). LS 10 rounds the corners of the basic scheme to form a near-elliptical scheme (area and offshore distance are unchanged); 2) layout schemes of different island filling area types: LS 3 reduces the island filling area of the basic scheme from 24 km^2 to 10 km^2; the offshore distance is approximately 4.6 km. LS 4 rotates LS 3 appropriately; the trend is parallel to the mainstream direction; 3) layout schemes of different offshore distance types, layout schemes 5, 6, 7, 8, and 11 are approximately 5.6, 7.1, 10.6, 9.1, and 4.1 km offshore, respectively.

5.2.1 Analysis of the impact of different arrangements of artificial island on the evolution of shore beach

To explore the influence of different offshore artificial island arrangements on the sandy coastal dynamic sediment environment and shoreline, this study set different offshore distances and artificial island arrangements with different plane forms (Fig. 10). First, the artificial island scheme is appropriately rotated so that the orientation is basically parallel to the mainstream direction, with the aim of reducing the corresponding flow blocking of the artificial island. Second, the artificial island is opened (opening distance of 1 km) to reduce the shadowing effect of SSE-waves. Lastly, the offshore distance is increased, and the artificial island is moved 2.5 km seaward. In this way, the offshore distance reaches 5.6 km, reducing the influence of the artificial island on the near-shore tide and waves. The LITLINE model was used to simulate shoreline changes after the implementation of the artificial island project with each arrangement. The results of the shoreline changes after 10 years of implementation are shown in Fig. 8. The following section describes the effects of each arrangement on the dynamic sediment mechanism and scouring of the shoreline on the east and west sides of the artificial island.

1) The changes in the dynamic field after the rotation of the artificial island indicate that the size of the water blocking section was reduced by approximately 7% compared to that in the artificial island scheme, causing a negligible amount of tidal dynamic impact. The impact on the near-shore tidal dynamics tended to be smaller, but the SSE- and SSW-wave shadowing effects were further enhanced. In addition, the wave effect in the shore section near Tianyahaijiao and Nanshan was enhanced, and the shoreline changes after the implementation indicated that the sand accumulated outward in the headland area of Taling. The shoreline change after implementation indicates that the outward accumulation of sand in the area of the Taling headland was significantly reduced compared to that in the artificial island project. The

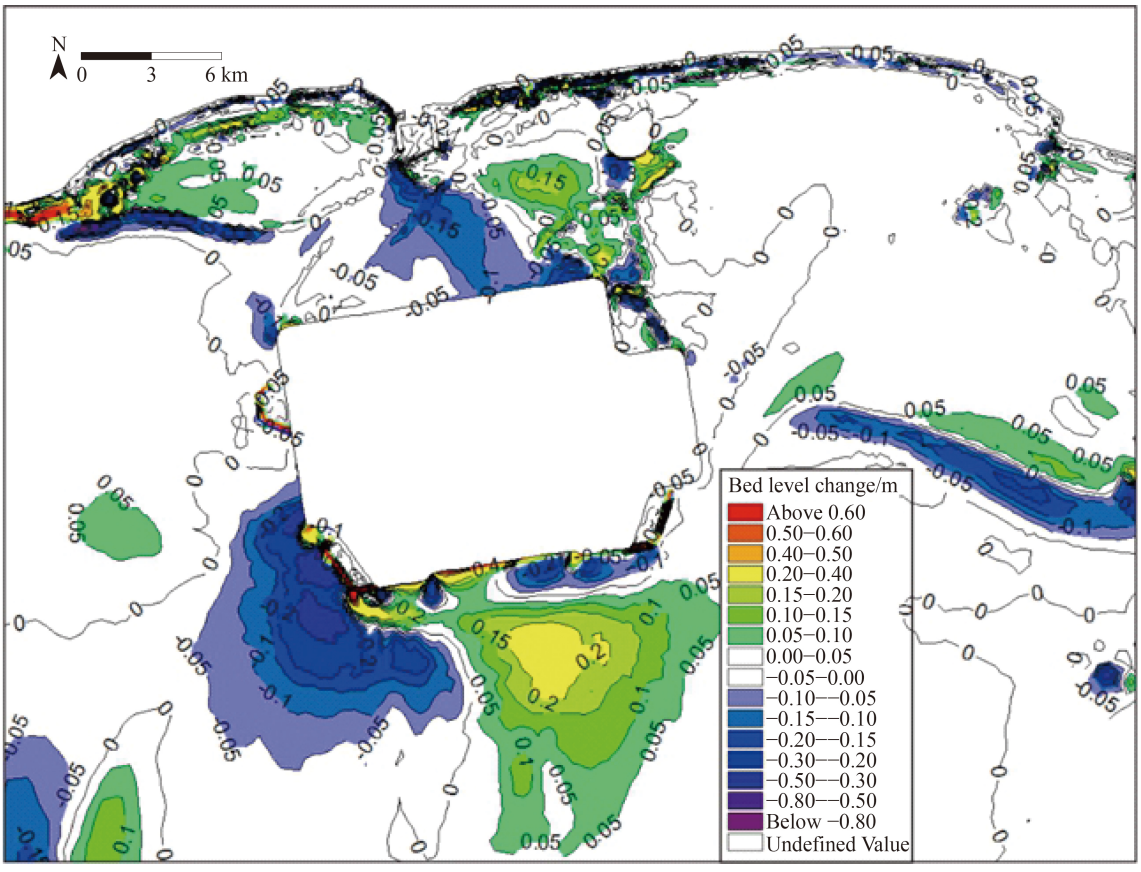

Fig. 8 Changes in regional erosion and deposition after the construction of artificial islands (Waves with 300-year return period in south-west direction, Chen, 2016)

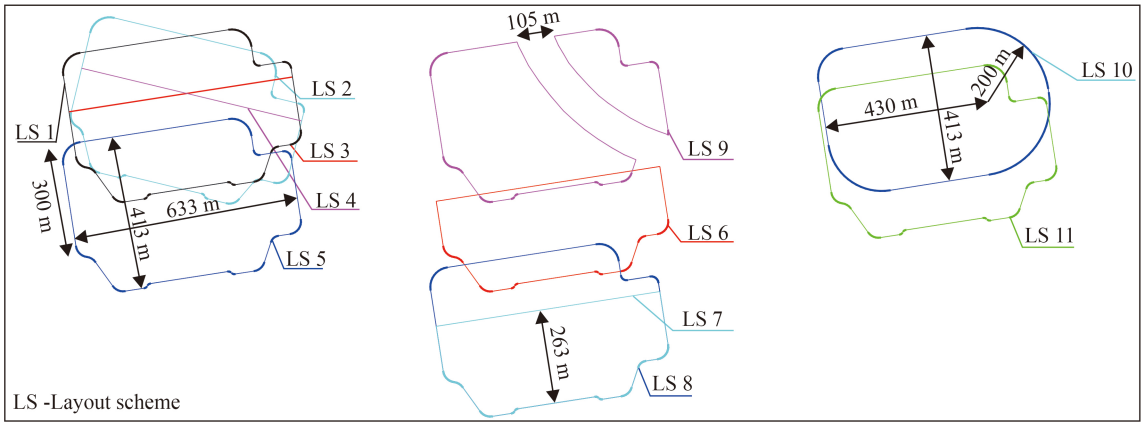

Fig. 9 Layout types of artificial islands.

shoreline was retreated approximately 60 m from the land side. The outward accumulation of sand in the rear of the Nanhai Guanyin artificial island was increased compared with the artificial island project, and the shoreline was extended to approximately 25 m outward. In addition, the scouring retreat in the shore section from Tanyao Port to Tianya Town was mitigated to some extent, while the scouring retreat in the shore section from Tianya Town to Tianyahaijiao was further strengthened. The retreat on the west and east sides of Nanhai Guanyin Island was enhanced, indicating that the shoreline change and the change in the dynamic sediment regimen by shore beach is compatible.

2) The change in the dynamic field after the opening of the artificial island indicates that some SSE-waves propagated from the deep sea to the near shore through the opening. While the artificial island weakened the shadowing effect of SSE-waves, it had no effect on the shielding of SSW waves. The results of the shoreline change after the implementation indicate that the outward

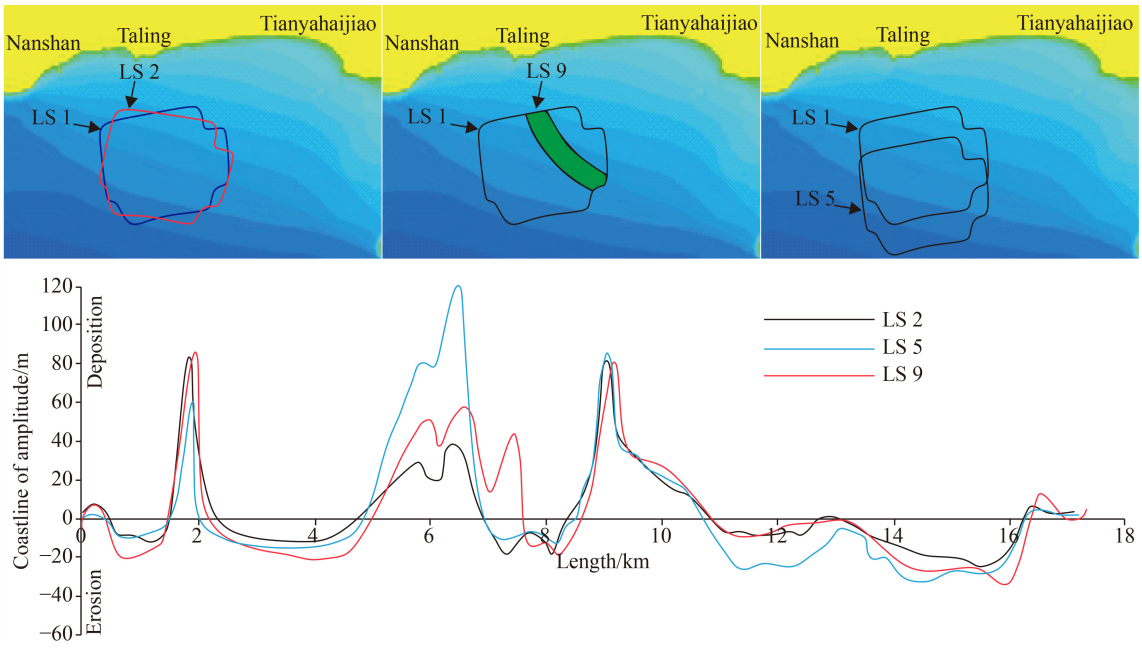

Fig. 10 Simulation results of shoreline changes after the implementation of different arrangements of offshore artificial islands.

accumulation of sand in the Taling headland area was significantly reduced compared to that in the artificial island scheme. In addition, the scouring retreat of the shore section from Danyou Port to Tianyahaijiao has been alleviated to some extent. The retreat of the west and east sides of Nanhai Guanyin Island was reduced, but the reduction was less than that of Tianyahaijiao.

3) The change in the dynamic field after increasing the offshore distance indicates that because the location of the artificial island is relatively far away from the shore of Tianyahaijiao and Nanshan, the influence on the near-shore tidal dynamics was further weakened along with the weakening of the SSE- and SSW-wave shadowing. However, no evident changes were observed in the flow and dynamic patterns of the flow field in the sea area. The shoreline changes after the implementation indicate that increasing the offshore distance had a certain inhibitory effect on relieving the scouring and retreating of the shoreline of Tianyahaijiao and Nanshan. Furthermore, the influence on the evolution of scouring and siltation of the Hongtang Bay shoreline was reduced, but the dynamic sediment pattern of the shoreline of Hongtang Bay did not change significantly. In addition, limited scouring alleviation was observed in the shoreline on the east and west sides of the artificial island.

Wave action is the controlling driving force of the near-shore sediment movement in Hongtang Bay. The influence of artificial island implementation on shore beach scouring and siltation is also realized by changing the propagation of the near-shore wave field. From the sediment dynamics mechanism of the impact of different arrangements on shore beach scouring and siltation evolution trends, the dynamics were similar to the overall distribution of scouring and siltation. Both show a certain range of scouring on the east and west sides of the artificial island covered area and siltation in the artificial island covered area. For the shore beach on the east side of the artificial island, the implementation of the artificial island creates cover for waves in the S, SSW, and SSW directions in this shore section, resulting in a relative increase in wave action in the deviated SE direction. Thus, scouring was observed in the net longshore sediment transport westward of this shore section. For the shore beach near the west side of the artificial island, the implementation of the artificial island creates cover for waves in the S, SSE, and SE directions in this shore section. The wave diffraction in the center of the artificial island causes increased longshore sediment transport capacity from west to east along this shoreline, and a scouring trend will be formed along this shoreline.

5.2.2 Impact of different arrangements of artificial island on shoreline evolution

The beach is altered after the implementation of the artificial island project (Fig. 11), in terms of the degree of scour mitigation of sensitive target beaches (Tianyahaijiao and Nanshan Temple Scenic Areas) by each LS, compared to the background LS.

1) The difference between the turning angle or partial round corners (LS 2 and LS 10) and the background LS (LS 1) is not significant, because the two schemes have a similar degree of influence on the overall shielding of waves.

2) Reducing the area or increasing the offshore distance (layout schemes 3, 4, 5, 6, 7, and 8) has a certain suppressing effect in alleviating the scouring recession of

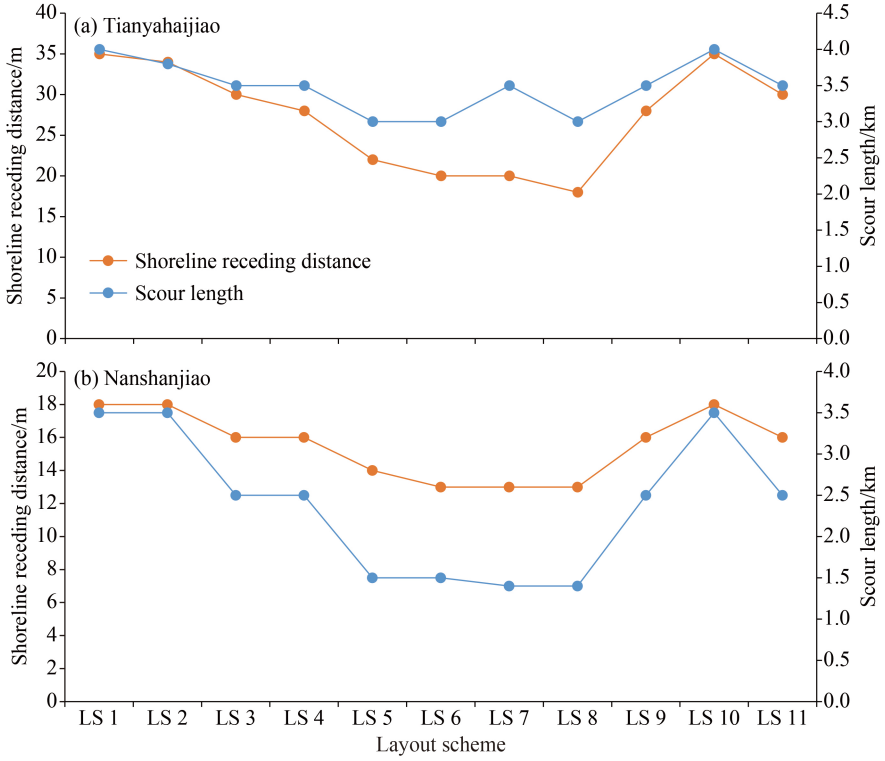

Fig. 11 Relationship between shoreline erosion length and maximum distance of shoreline erosion caused by different types of artificial island construction.

sensitive target beaches. The smaller the area of the artificial island, and the farther the offshore distance, the less significant the impact on the beach tends to be, among which LS 8 (with the smallest area and farthest offshore distance) has the least significant impact on the nearby beach. After 10 years of implementation, the maximum scouring amplitude of the Tianyahaijiao scenic area was approximately 18 m, and the maximum scouring of the Nanshan scenic area was less than 13 m.

3) Opening (LS 9) has a certain suppressing effect in alleviating the scouring recession of sensitive target beaches; however, the degree of suppression is significantly limited.

From the perspective of the beach scouring impact after the implementation of the artificial island scheme, the dynamic sediment mechanism of the impact on the beach and the overall distribution of scouring and silting are similar for all schemes, which show scouring to the east and west of the shielding area of the artificial island to some extent, and silting in the shielding area of the artificial island. Compared with the background scheme, each scheme has a certain suppressing effect in alleviating the scouring recession of sensitive target beaches.

5.3 Comparative analysis of the influence of artificial island construction on beach evolution

The effect of artificial islands on beaches (Fig. 12; Lepetit and Moreau, 1976) is essentially similar to that of offshore dikes. In the wave shadow area behind the breakwater, sedimentation is triggered by the weakening of dynamic forces, and beach erosion is caused by strong dynamic forces on both sides of the breakwater (Zhu et al., 2019).

Before the construction of the west artificial island of the Hambantota Port Phase II Project, the sedimentation intensity in the entrance area of the breakwater was approximately 1.0 m/y and that in the inlet channel was approximately 0.4 m/y. After the construction of the west artificial island, the sedimentation intensity in the entrance area and inlet channel decreased to 0.69 and 0.27 m/y, respectively (Xu ang Zhang, 2019). The impact of the proposed artificial island for the new Sanya airport on the beaches decreased with the distance from the artificial island, and its impact was relatively significant in waters 10 km away (Tan and Gao, 2019). The frontier waters on the north and south sides of the Xiutu artificial island in Quanzhou Bay were substantially altered. The deposition intensity on the south side increased, and a deposition intensity of 20 cm/y emerged near the front coastline. Although the deposition intensity on the north side of the artificial island near the Big Island increased from 10 cm/y before the project to 15 cm/y, the range of 10 cm/y deposition intensity on the west side increased as well (Huang, 2019).

The beaches in the wave shadow area of Sun Island, Hainan Province, were silted up. In 2016, the tombolo was formed with a total width and length of 370 and

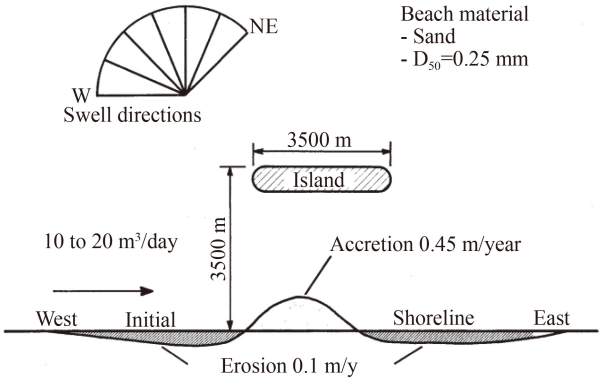

Fig. 12 Schematic diagram of the impact of artificial islands on beaches (Lepetit and Moreau, 1976).

1500 m, respectively (Li et al., 2019b). The north-east side of the Sun Island was eroded by wave refractions and diffractions after the construction of Sun Island. The maximum erosion width and length were approximately 20 and 380 m, respectively. There was a severe erosion retreat on the south-west side of the Sun Island, with a width and length of approximately 40 and 2000 m, respectively. To the west of the vertical coastal projection of the Riyuewan artificial island in Hainan Province, the coastline was eroded owing to wave reflection. The maximum erosion width was approximately 4 m (8 m after 2 years), and the total erosion length was 1 km (1.3 km after 2 years). In the main wave shadow area, deposition occurred in the shoreline. The maximum deposition width was approximately 32 m (72 m after two years), which occurred in waters approximately 30 m to the east of the connecting bridge. The length of the deposition area was approximately 869 m (943 m after two years). To the east of the deposition area, the coast was eroded; the maximum erosion width was less than 3 m (5 m after 2 years), while the erosion length was approximately 937 m (Zhang et al., 2016). In this study, after constructing the artificial island, the maximum scouring distance was 14–37 m, and the scouring length was 1.5–4.2 km. The influence of different types of artificial island constructions on beaches was different. It is necessary to enhance topographic monitoring after the construction of an artificial island, and further analyze the impact of this construction on beach erosion and deposition. This study provides a reference for the impact of global coastal artificial island construction on beaches.

It further supplements current research on foreign beach and the impact of artificial islands. We attempted to establish the threshold of artificial island construction and shoreline impact; however, the impact of artificial islands in each region is not the same. The purpose of our research, with the construction of artificial islands on the sandy coast of Hongtang Bay in the South China Sea as the object, was to determine (i) which artificial islands layout has the least impact on the shoreline, and (ii) the relationship between the different types of artificial islands layout.

6 Conclusions

1) The entire shoreline of Hongtang Bay exhibits a dynamic trend of slowed scouring and receding. After the implementation of the offshore artificial island, the sea area at Tianyahaijiao on the east side of the artificial island was primarily subject to the action of waves in the SSE direction. The sea area at the Nanshan Scenic Area on the west side of the artificial island was primarily subject to the action of waves in the SSW direction, thereby leading to changes in coastal sediment transport and beach deformation.

2) Based on the LITLINE model, the shoreline alterations under the layout of decreasing the area of artificial island filling (the projection length of the main wave to the crest line), and increasing the offshore distance were calculated respectively, and under a similar artificial island form, the impact of its construction on the beach increased with an increase in the projection length of the main wave of the artificial island to the crest line. In addition, the impact of artificial island construction increased as the offshore distance decreased.

3) The greater the distance of offshore engineering from the shoreline, and the smaller the area of the artificial island layout scheme, the greater the advantage, which can alleviate the adverse effects of the artificial island on the near-shore beach; however, the layout schemes of artificial islands on sandy coasts should also consider the traffic environment, channel safety, landscape, and ecology.

Acknowledgments This study was funded by the National Natural Science Foundation of China (Grant No. 51979132); State Key Laboratory of Hydraulic Engineering Simulation and Safety (Tianjin University) (No. HESS1719); Fundamental Research Funds for Central Welfare Research Institutes (Nos. TKS190406, TKS20200312 and TKS190405).

References

Amrousi M E, Elhakeem M, Paleologos E (2019). Building on water: the use of satellite images to track urban changes and hydrodynamic models to simulate flow patterns around artificial islands. In: Proceedings of the 2nd International Conference on Intelligent Human Systems Integration (IHSI 2019): Integra. Cham: Springer

Chee S Y, Othman A G, Sim Y K, Adam A N M, Firth L B (2017). Land reclamation and artificial islands: walking the tightrope between development and conservation. Glob Ecol Conserv, 12: 80–95

Chen G (2016). Mathematical model of tidal current and sediment for artificial island project of Sanya New Airport. Dissertation for the Doctoral Degree. Nanjing: Hohai University (in Chinese)

DHI (2012). LITLINE - Coastline Evolution, LITLINE User Guide. Horsholm: Danish Hydraulic Institute

Fan Y, Pan J, Wang H (2019). Numerical study of the wave design for the artificial island of Hong Kong-Zhuhai-Macao bridge while considering the extreme weather I: selection method of the typhoon

track in numerical wave simulation. Adv Water Sci, 30(6): 126–135

Gao S, Collins M (1992). Net sediment transport patterns inferred from grain-size trends, based upon definition of “transport vectors”-reply. Sediment Geol, 81(1−2): 47−60

Hou X, Wan H, Ting W (2016). Shape changes of major gulfs along the mainland of China since the early 1940s. Acta Geogr Sin, 71(1): 118−129 (in Chinese)

Hou Q, Zuo L, Lu Y, Wang Z, Mo S, She X (2017). Hydrodynamic environment response to human interventions in a Macro tidal bay: the example of the Quanzhou Bay. J Basic Sci Eng, 25(6): 1124-1128 (in Chinese)

Huang Z (2019). Impact of Xiutu artificial island construction on surrounding water and sediment conditions in Quanzhou Bay. Port Waterway Eng, 564(12): 32−38 (in Chinese)

Kuang C P, Jiang L F, Ma Y, Qiu R F (2019). Wave-current coupled hydrodynamic responses to artificial island and beach nourishment projects. J Tongji U (Natural Science), 47(1): 42−50 (in Chinese)

Li H, Zhang H, Xia W, Yu H, Xu Y, Liu X, Zhang Y (2019a). Influence on the sandy coast evolution of the ocean engineering–a case study of artificial Riyue island, Wanning city, Hainan Island. Mar Environ Sci, 38(4): 17−23 (in Chinese)

Li X (2017). Influence of offshore artificial island on sandy coastal evolution. Dissertation for the Doctoral Degree. Qingdao: First Institute of Oceanography, State Oceanic Administration (in Chinese)

Li Y, Gang L, Feng C, Qi H, Zhu J (2019b). Study on the influence of hard revetment, harbor engineering and artificial island on the adjacent beach in China. J App Oceanogr, 38(1): 118−125 (in Chinese)

Lepetit J P, Moreau S (1976). Study of an artificial island. In: Division Hydraulique Maritime-Laboratoire National d'Hydraulique Electricite de France-Chatou-France

Lu Y, Ji R, Zuo L (2009). Morphodynamic responses to the deep water harbor development in the Caofeidian sea area, China’s Bohai Bay. Coast Eng, 56(8): 831–843

Luo S, Liu Y, Jin R, Zhang J, Wei W (2016). A guide to coastal management: benefits and lessons learned of beach nourishment practices in China over the past two decades. Ocean Coast Manage, 134: 207–215

Ma B, Dai Z, Pang W, Ge Z, Li S, Mei X, Huang H (2019). Dramatic typhoon-induced variability in the grain size characteristics of sediments at a meso-macrotidal beach. Cont Shelf Res, 191: 104006

Pang W, Ge Z, Dai Z, Li S, Huang H (2021). The behaviour of beach elevation contours in response to different wave energy environments. Earth Surf Process Landf, 46(2): 443–454

Prasad R, Nair L S, Kurian N P, Prakash T N (2020). Shoreline evolution along a placer mining beach of south-west coast of India. J Coast Res, 89(1): 150–157

Rabionet I C, García V G, Galindo M R (2008). Indicators for evaluating the impact of artificial islands on the Barcelona Coast. Coast Manage, 36: 254–273

Sheng T, Sun D, Yang Z (2016). Analysis of artificial island construction influences on individual flood erosion and deposition in estuary. J Waterway Harbor, (1): 18−26 (in Chinese)

Shi P, Cao L L, Mo W Y, Xie J (2015). Influence of man-made island construction on the stability of the beach in the west coast of Haikou Bay. J Trop Oceanograph, 34(5): 57–63

Shu G, Michael C (1994). Net sediment transport patterns inferred from grain-size trends, based upon definition of “transport vectors”-reply. Sediment Geol, 90(1): 157–157

Su Q, Peng C S, Yi L, Huang H H, Liu X Y, Xu X Y, Chen G G, Yu H J (2016). An improved method of sediment grain size trend analysis in the Xiaoqinghe Estuary, southwestern Laizhou Bay, China. Environ Earth Sci, 75(16): 1–10

Sun J, Zhan We H, Yao Y T, Liu S J, Feng Y C (2015). Current situation and influence factors of coastal erosion in Guangdong. Acta Oceanol Sin, 37(7): 142−152 (in Chinese)

Tan X, Jian G (2019). Impact of the Sanya new airport artificial islands project on tidal dynamics of the Hongtang Bay. Mar Sci Bull, 21(2): 1–15

Walker D J, Rana M Y (1999). Modelling coastal processes on sandy beaches. In: Modelling Coastal Sea Processes: 317–341

Wang C, Min C, Qi H, Intasen W (2020). Grain-size distribution of surface sediments in the Chanthaburi Coast, Thailand and implications for the sedimentary dynamic environment. J Mar Sci Eng, 8(4): 242

John W D, Yunus R M (1999). Modelling coastal processes on sandy beaches. Modelling Coastal Sea Processes: 317–341

Wang C, Zhang Q, Xin H (2012). Longshore sediment transport due to Guang’ao breakwater project of Shantou port and its effect on Haojiang estuary. Port Waterway Eng, (1): 6−11 (in Chinese)

Xu R, Jun Z (2019). Impact of Hanbantota Port phase II west artificial island scheme on beach evolution. Port Waterway Eng, 560(9): 89−94 (in Chinese)

Yang F, Pan J N, Wang H C (2019). Numerical study of the wave design for the Artificial Island of Hong Kong-Zhuhai-Macao bridge while considering the extreme weather: I: selection method of the typhoon track in numerical wave simulation. Adv in Water Sci, 30(6): 126–135

Yue N, Jiang W, Zhu L, Ma F (2008). Impact of man-made off-coast island on sandy coast. Mar Geo Lett, 24(4): 18−22 (in Chinese)

Zhang M, Wu W, Li C, Chen L, Fan S G (2011). On the construction of crescent-shaped artificial island in Jiangsu Province. Ocean Develop Manag, (3): 30−33 (in Chinese)

Zhang C, Jia H, Zheng Z, Li L, Li N, Wang P, Xie J (2016). Countermeasures and analysis on the positive and negative environmental effect of offshore artificial island reclamation——a case study of artificial island project of Riyue Bay Hainan. Transact Ocean Limn, (2): 17−23 (in Chinese)

Zhao D (2014). Study on the sandy beach erosion and protection technology of the offshore artificial sand bar. Dissertation for the Doctoral Degree. Qingdao: Ocean University of China (in Chinese)

Zhu J, Cai F, Shi F, Qi H, Liu J, Cao H, Zheng J (2019). Beach response to breakwater layouts of drainage pipe outlets during beach nourishment. Estuar, Coastal Shelf Sci: 228(354): 106354.1–106354.13

Zuo S, Biao L (2016). A Special Research Report on Beach Evolution Analysis of Sanya New Airport Artificial Island Project. Tianjin: Tianjin Research Institute of Water Transportation Engineering (in Chinese)